*Faraday Discuss.*, 1992, **94**, 317–327

# Scanning Tunnelling Microscopic Investigation of Iodine-covered Pt Single-crystal Electrodes

**Helmut Baltruschat, Ulrich Bringemeier and Roland Vogel**

*Institute of Physical Chemistry, University of Witten/Herdecke, Stockumer Str. 10, 5810 Witten, Germany*

Using a home-built scanning tunnelling microscope (STM), the structure of iodine adlayers in air and in electrolyte has been investigated. In air, the occurrence of tip–adatom interactions was demonstrated and an antiphase domain boundary was resolved atomically. The adlayer structure on the Pt(100) surface in $10^{-4}$ mol dm$^{-3}$ $I^-$ solution (pH 4) is potential dependent. At 0.75 V *vs.* RHE the Pt(100) $(\sqrt{2}\times 5\sqrt{2})R45°-I$ adlattice is found. At 0.5 V, domains of this structure and of a Pt(100) $(\sqrt{2}\times\sqrt{2})R45°-I$ adlattice exist. Desorption of iodine (at 0.25 V) leads to a hexagonally reconstructed surface. During deposition of small amounts of copper onto the iodine-covered surface, islands with diameters between 10 and 30 Å, which are one to three atomic layers high, are formed first and then coalesce to a hill-like structure.

Iodine adlattices are an interesting model adsorbate on surfaces of the Pt-group metals due to their stability even in ambient atmosphere. Adsorbed iodine is also of some technological interest since it serves as an efficient corrosion inhibitor for less noble metals.

Smooth, well ordered Pt and Rh surfaces can be prepared for the low-index faces by annealing the crystal in iodine vapour.[1,2] This has also been verified by STM.[3–5] In the case of Pd, a smooth (111) surface is even generated from an electrochemically roughened one by simply adsorbing iodine from electrolyte at room temperature.[6]

Adsorbed iodine can then be desorbed in an electrochemical cell either by displacing it with CO (followed by the electrochemical oxidation of the adsorbed CO) or by cathodic desorption in an alkaline solution. As compared to other methods of single-crystal electrode preparation (quenching of the annealed crystal in pure water or cooling in an Ar atmosphere,[7,8] this method offers the advantage that the surface is not susceptible to contamination during mounting of the crystal in an electrochemical cell.

The adlattice structure of these surfaces using *in situ* STM has been reported for the Pt(111) and the Pt(100) surface,[4,9,10] thus confirming former *ex situ* LEED results:[11,12] on Pt(111), three iodine adlattices have been identified depending on potential and pH: a $(3\times 3)-I$, $\Theta=0.44$, a $(\sqrt{7}\times\sqrt{7})R19°-I$, $\Theta=0.43$ and, at more negative potentials, a $(\sqrt{3}\times\sqrt{3})-I$, $\Theta=0.33$ adlattice. At Pt(100), a $(\sqrt{2}\times 5\sqrt{2})R45°-I$ addlatice ($\Theta=0.6$) was found; the potential dependence of iodine adsorption was not investigated for this Pt face. Interestingly, two different orientations with respect to the substrate lattices were found in air by STM for the Pt(111)$(3\times 3)-I$ [3] and Pt(100) $(\sqrt{2}\times 5\sqrt{2})R45°-I$.[5]

## Experimental

Our home-built STM (Fig. 1) is derived from the 'beetle type' construction of Besocke and co-workers.[13,14] It was modified to minimize the number of electrical connections to the moving parts and, of course, for use in electrochemistry.

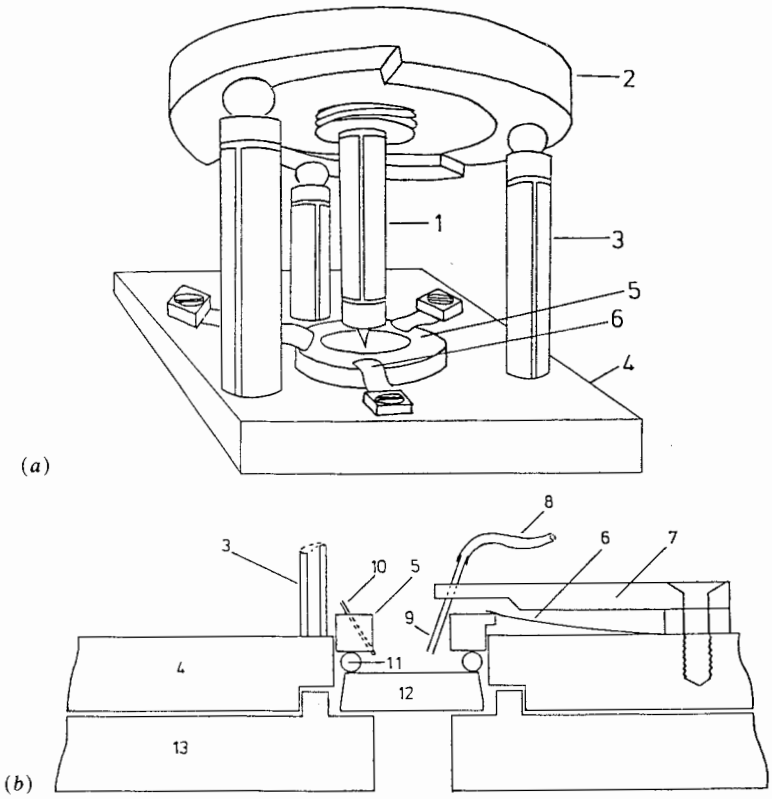


**Fig. 1** Modified 'beetle-type' STM. (*a*) Perspective view of STM head; (*b*) section through electrochemical cell 1, single tube scanner with tip; 2, scanner support disk (ramp slider); 3, ball-bearing carrier piezo; 4, STM base plate; 5, Kel-F cell; 6, leaf spring; 7, PTFE cantilever; 8, fluid line; 9, counter-electrode (Pt tube); 10, reference electrode (Pt wire); 11, Kalrez O-ring; 12, sample; 13, sample support plate. (Reprinted with permission from ref. 4.)

A coarse approach is achieved using the inertial slider principle. The three ball-bearing outer piezos (3), which support the scanner support disk (2), are quickly moved tangentially in one direction and then slowly moved back to their original position. Because of inertia, the disk (2) only follows the slow movement. Repeating this process results in a rotation of the disk. Ramps machined into this disk translate this rotation into a vertical movement of the scanner and hence the tip. This allows movement of the tip to or from the sample.

The tip can be scanned in $x$, $y$ directions by applying appropriate voltages to the four outer electrodes of the scanner piezo. For a vertical movement a voltage between all outer electrodes and an inner electrode is applied.

The piezo constants were evaluated to within 10% using HOPG graphite. For every new tip, exact calibration factors were determined from the Pt(100) $(\sqrt{2}\times 5\sqrt{2})$R45°−I adlattice in air. These were used for the determination of lattice constants and atomic distances, but not for the representation of the data in the figures.

The cell (diameter 6 mm) consists of a Kel-F cylinder and a Kalrez O-Ring which are spring loaded against the sample surface. This gives a cell volume of 150 μl. The sample (1 cm diameter and 3 mm thick) can be easily exchanged by lifting the STM base plate. Electrolyte is introduced into this cell through a PTFE tube ending in a piece of Pt tube, which is fixed at a PTFE cantilever. This Pt tube also serves as

counter-electrode. The end of a small Pt wire fixed in a bore of the Kel-F cylinder as a dynamic hydrogen reference electrode by continuously evolving a small amount of $H_2$.

The STM is mounted as usual on a Viton damped stack of metal plates and is enclosed in a Plexiglass housing, which serves for thermal isolation and allows measurements under inert-gas atmosphere.

Our electronics consists of an $I-V$ converter which is incorporated in the STM head, the usual feedback loop based on a logarithmic amplifier and an integrator, a digital scan generator and a +100 V final stage. A compensation voltage applied to the outer piezos prevents high d.c. levels at the scanner electrodes. Data acquisition and control of the instrument are performed by a PC 386-20 with STiMage software from RHK Technology, Rochester Hills, USA. Computer and electronics are interfaced *via* a DT 2821-F interface board from Data Translation, Marlboro, USA. The scan generator was designed to emulate the RHK STM 100-3 electronics from RHK Technology.

A home-built bipotentiostat and function generator are connected to the STM circuitry, the working electrode being at true ground.

Tips were etched from either W or Pt–Ir wire (0.25 mm) and insulated with epoxy resin. Owing to the surface tension of the resin the very tip remains uncoated. Annealing at 80 °C for 2 h ensures that the epoxy coating is stable and clean enough to be no source of contamination in the electrochemical cell.

The Pt(111) single crystal was purchased from Goodfellow, Cambridge, UK, and oriented and polished to within ±0.2° by the KFA Jülich, Germany. The Pt(100), oriented to within ±0.25°, was purchased from Kristallhandel Kelpin, Leimen, Germany.

Prior to STM experiments the sample was heated in a hydrogen flame to *ca.* 1000 K for a few minutes. The hot crystal was then transferred into a flask purged with nitrogen or argon and containing some iodine crystals.

For the *in situ* imaging of the iodine adlattices, an iodide-containing electrolyte was used in order to enable an equilibrium between dissolved and adsorbed iodine ($10^{-4}$ mol dm$^{-3}$ KI, $10^{-4}$ mol dm$^{-3}$ $HClO_4$, $10^{-2}$ mol dm$^{-3}$ $NaClO_4$). Since this electrolyte is not buffered, the reference potential of the dynamic hydrogen electrode corresponds to hydrogen evolution from water, *i.e.* to an RHE at *ca.* pH 11. For the Cu deposition experiments, $10^{-3}$ mol dm$^{-3}$ $Cu^{2+}$ in $10^{-2}$ mol dm$^{-3}$ $H_2SO_4$ was used. A Cu wire was used as reference electrode in these experiments.

## Results and Discussion

Images of the iodine adlattice present on the Pt(111) and Pt(100) surface after the iodine treatment described in the Experimental section are shown in Fig. 2 and 3. Those two images have been chosen here since they demonstrate the ability of STM to reveal real-space structures such as defects; typically images are obtained which do not show these defects.

In Fig. 2 two domains of the Pt(100) $(\sqrt{2}\times 5\sqrt{2})$R45° adlattice with the characteristic double-row structure are seen. Every third row of iodine atoms is invisible because they are placed in fourfold hollow sites of the substrate lattice.[5] These two domains are separated by an antiphase domain boundary which shows up as a triple row.

In Fig. 3, an image of one of the Pt(111) $(3\times 3)-I$ adlattices is presented. Here, every fourth iodine atom is situated 'on top' of Pt atoms and therefore appears bright in the image, the other three are at bridge sites. (One of these, situated in the scan direction between the 'on top' iodine atoms, is only visible as a shadow due to a non-optimized feedback control.) In the upper right-hand corner, one of the bright atoms is not at its regular position. Interestingly, its actual position depends on the scan direction of the tip. We have to assume, that one of the adlattice atoms is missing, and therefore another atom is able to move between two 'on top' sites, to which it is forced by the interaction with the tip.

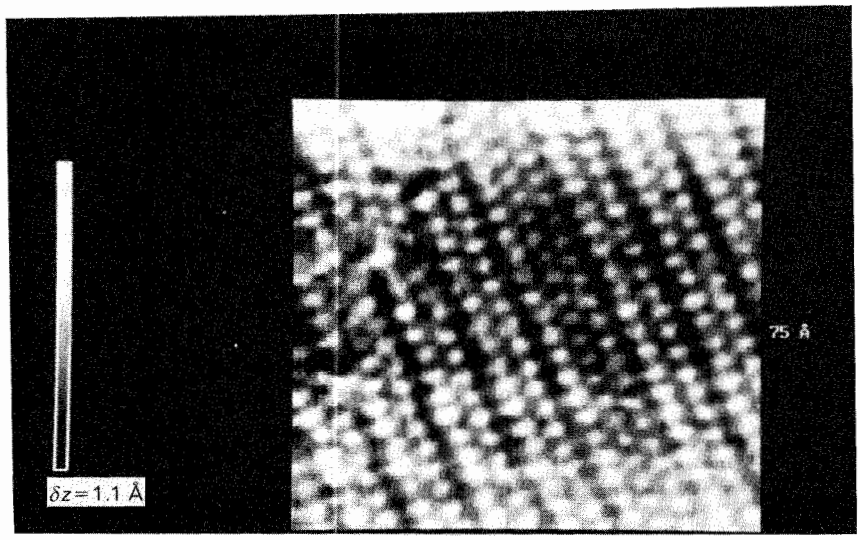


**Fig. 2** Topographic image of the Pt(100) $(\sqrt{2}\times 5\sqrt{2})$R45° − I adlattice in air. Tip bias = −4 mV, constant current = 5 nA. Scan area 7.5 nm × 7.5 nm, scanning speed 251 nm $s^{-1}$. Note the triple row in the middle due to the domain boundary

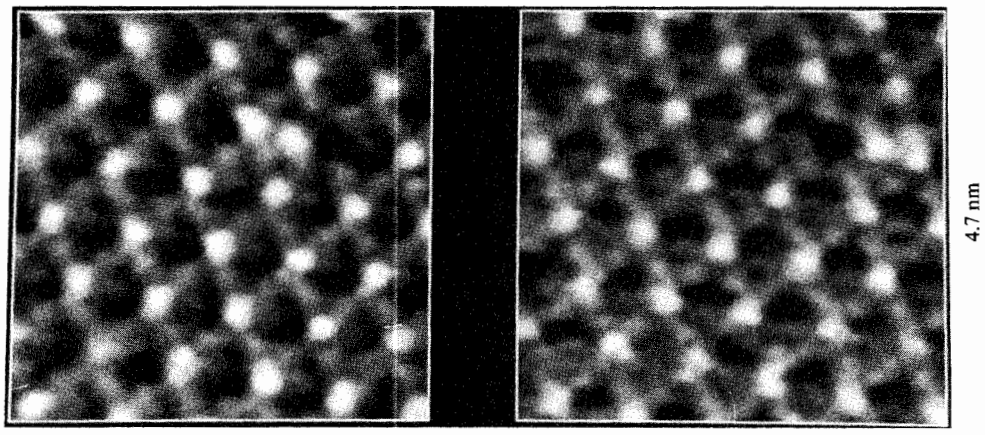


**Fig. 3** Current image (constant height mode) of the Pt(111) (3 × 3) − I adlattice in air. Tip bias −4 mV, $T_t$ = 10 nA, scan area 4.7 nm × 4.7 nm, scanning speed 550 nm $s^{-1}$. Note the defect in the upper right-hand corner

In solution, adsorbed iodine also forms the $(\sqrt{2}\times 5\sqrt{2})$R45° adlattice on the Pt(100) face the rest potential (1 V). Fig. 4 shows a topographic image together with a cross-section parallel to the longer unit-cell vector. Qualitatively, the result is in accordance with what one would expect from the model. However, the total height variation (1 Å) is larger than expected from a simple hard-sphere model, in which the difference in height between the iodine atoms in fourfold hollow sites and the 'nearly on top' sites is *ca.* 0.6 Å. Electronic effects therefore also might play a role.

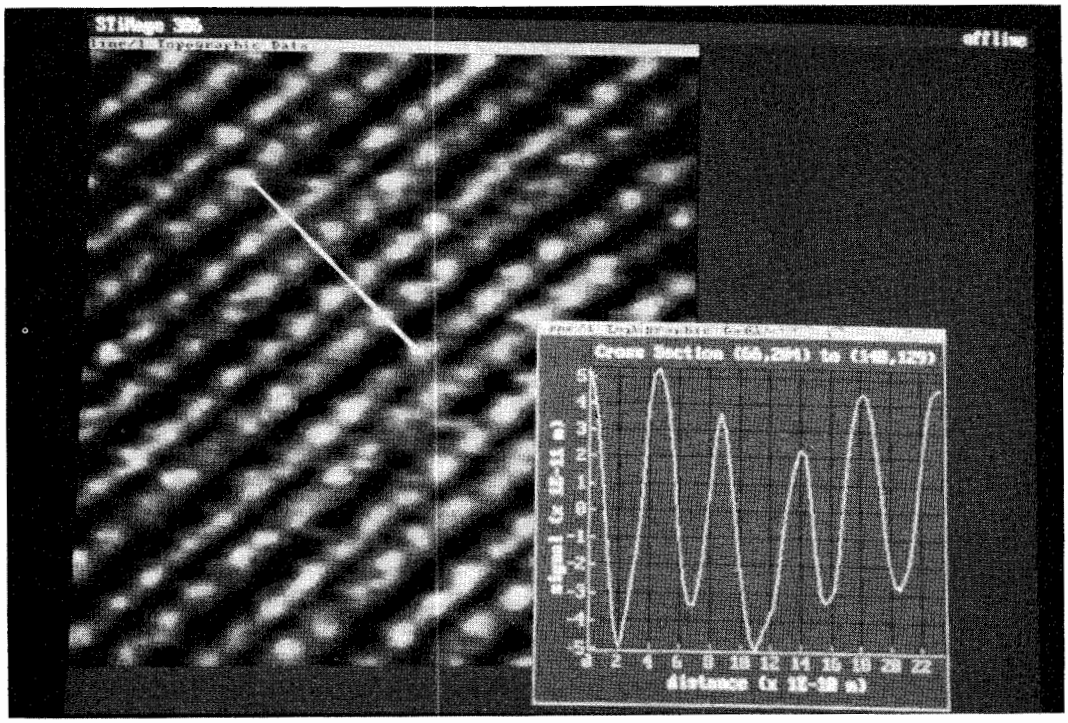

**Fig. 4** Topographic image (constant current mode) of Pt(100) $(\sqrt{2}\times 5\sqrt{2})$R45°−I, measured *in situ* in $10^{-4}$ mol dm$^{-3}$ KI, $10^{-2}$ mol dm$^{-3}$ $NaClO_4$, $10^{-4}$ mol dm$^{-3}$ $HClO_4$ at 0.75 V *vs.* RHE, tunnelling voltage −3 mV; scan area 6 nm × 6 nm, scan speed 400 nm s$^{-1}$

By analogy to iodine adsorption on the Pt(111) electrode,[11] some of the iodine is expected to be desorbed at more negative potentials. We therefore examined the adsorbate structure after sweeping to 0.5 V. The result is shown in Fig. 5. Whereas in the upper part the characteristic double-row structure is still present, in the lower part a more quadratic structure can be seen with spacings between the atoms of 3.9 Å as expected for a $(\sqrt{2}\times\sqrt{2})$ adlattice. A corresponding lattice drawn through these atoms coincides with the $(\sqrt{2}\times 5\sqrt{2})$ double-row structure in the upper part. In Fig. 5(*b*), obtained under the same conditions, a quadratic $(\sqrt{2}\times\sqrt{2})$ structure also can be seen in the lower part of the image, whereas the upper part appears somewhat disordered.

This result of a Pt(100) $(\sqrt{2}\times\sqrt{2})$R45°−I adlattice ($\theta = 0.5$), a model of which is shown in Fig. 6, is at variance with the Pt(100) $(\sqrt{2}\times 2\sqrt{2})$R45°−I adlattice obtained for $\theta = 0.5$ from dosing with $I_2$ vapour under UHV and determined by LEED. However, we cannot yet exclude that this structure also exists at the electrode surface.

The low resolution of the images shown in Fig. 5 as compared to that of the $(\sqrt{2}\times 5\sqrt{2})$ lattice might be caused by the lower atomic density which allows the atoms to be more mobile and leads to more thermal movement. It is evident that for a good resolution in STM the position of the atoms must be fixed, which, under UHV, is achieved by using low temperatures.

Schardt and co-workers, however, were able to resolve the Pt(111) $(\sqrt{3}\times\sqrt{3})-$I, $\theta = 0.33$, adlattice *in situ*.[9] But compared to this hexagonal adlattice, the positions of the atoms in the $(\sqrt{2}\times\sqrt{2})$ [or the alternative $(\sqrt{2}\times 2\sqrt{2})$] adlattice are less fixed due to a lower symmetry: In the $(\sqrt{2}\times\sqrt{2})$ structure the symmetry is fourfold, but this adlattice is a very open structure. The $(\sqrt{2}\times 2\sqrt{2})$ adlattice is hexagonal, but highly distorted.

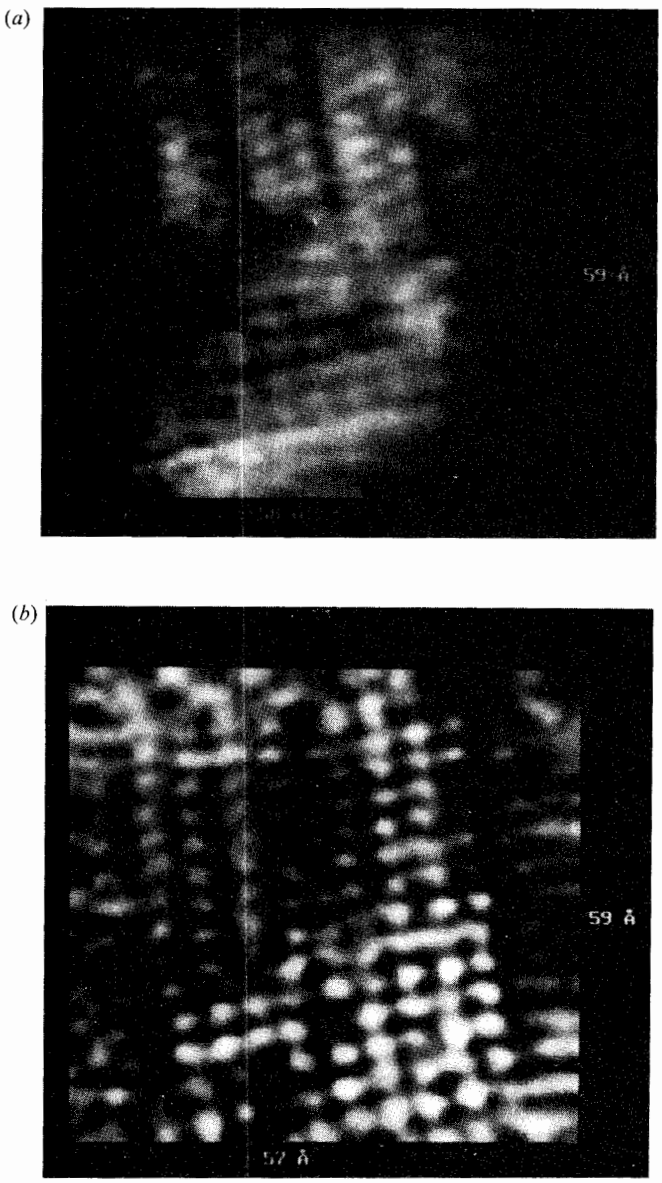


**Fig. 5** (*a*) Current image of the Pt(100) in $10^{-4}$ mol dm$^{-3}$ KI, $10^{-2}$ mol dm$^{-3}$ $NaClO_4$, $10^{-4}$ mol dm$^{-3}$ $HClO_4$ at 0.5 V, W, tip; tunnelling voltage −5 mV, scan area 5.8 nm × 5.8 nm, scan speed 575 nm s$^{-1}$. (*b*) Similar to (*a*), but topographic image, scan speed 287 nm s$^{-2}$

As visible from Fig. 6, atoms can be expected to move easily (or be easily moved by interaction with the tip), *e.g.* from a position belonging to one adlattice to one belonging to the other. The disorder in the upper half of Fig. 5(*b*) might be due to iodine atoms randomly occupying the twofold sites of the $(\sqrt{2}\times\sqrt{2})$ and $(\sqrt{2}\times 2\sqrt{2})$ structures.

In the model (Fig. 6), the iodine atoms were placed into bridge sites. Alternatively, the iodine atoms in the $(\sqrt{2}\times\sqrt{2})$ structure might also occupy top or fourfold hollow site positions. In principle, it should be possible to determine the absolute position, *e.g.* by using the $(\sqrt{2}\times 5\sqrt{2})$ domain in Fig. 5(*a*) to elucidate the substrate lattice. Owing

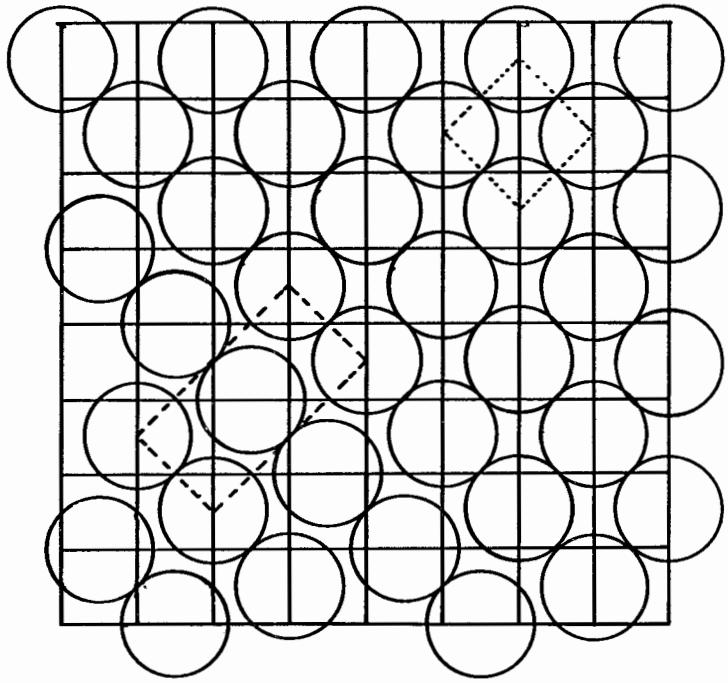

**Fig. 6** Model of a $(\sqrt{2}\times 2\sqrt{2})$ (lower left-hand side) and a $(\sqrt{2}\times\sqrt{2})$ (upper right-hand side) adlattice

to the limited digital resolution of 0.5 Å, the position of the substrate lattice at a distance of 50 Å (*i.e.* in the $(\sqrt{2}\times\sqrt{2})$ domain) is only defined to within 2.5 Å, *i.e.* nearly the substrate lattice constant.

At a potential of 250 mV we obtained the images shown in Fig. 7 with a hexagonal symmetry and atomic distances of 2.9 Å. We interpret this structure as being due to Pt atoms of the hexagonally reconstructed Pt(100) surface, $d = 2.8$ Å. This interpretation is supported by the finding of parallel streaks [with a spacing of *ca.* 15 Å, Fig. 7(*c*)] perpendicular to the scan direction at a different part of the surface, which are due to the mismatch between the topmost hexagonal lattice and the second layer of Pt atoms. (In the case of Fig. 7, these rows probably run parallel to the scan direction and therefore are not visible due to the feedback loop.)

A similar hexagonal reconstruction was found for the Au(100) electrode at low potentials.[15] In the case of the Pt(100) electrode, however, this reconstruction is astonishing: In the pH 4 solution, we would expect the iodine to be displaced by adsorbing hydrogen, which might be expected to lift the reconstruction.

Sometimes we also observed small domains of up to 10 atoms, where the structure and the atomic distances were indicative of an unreconstructed Pt(100) surface. This might be caused by the slowness of the reconstruction process.

Adsorbed iodine might also serve as a model for surface active compounds. Its technical use as a corrosion inhibitor has been mentioned in the introduction. We therefore performed some preliminary experiments on the initial stages of copper deposition onto the iodine-covered Pt(100) crystal (Fig. 8).

Fig. 8(*a*) shows the topography *in situ* before deposition. Clearly visible is a rectangular, monoatomic depression which is typical for the Pt(100) face.[5] During deposition at −200 mN (*vs.* $Cu/Cu^{2+}$) the tip was retracted by 100 nm in order to

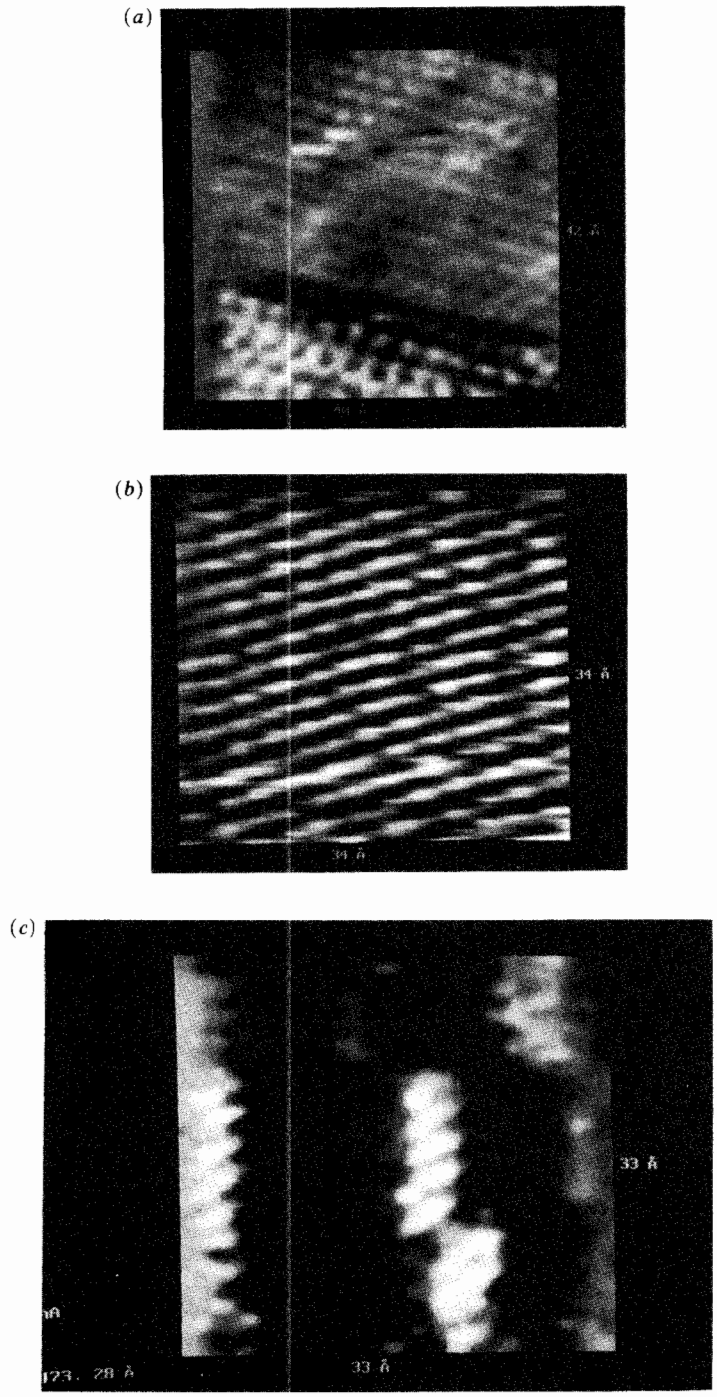


**Fig. 7** As Fig. 5, but at 0.25 V: (*a*) current image, tunnelling voltage −4 mV, scan area 4.0 nm × 4.2 nm, scan speed 397 nm $s^{-1}$. (*b*) Topographic image, tunnelling voltage −4 mV, scan area 3.4 nm × 3.4 nm, scan speed 396 nm $s^{-1}$. (*c*) Current image, tunnelling voltage −10 mV, scan area 3.3 nm × 3.3 nm, scan speed 410 nm $s^{-1}$

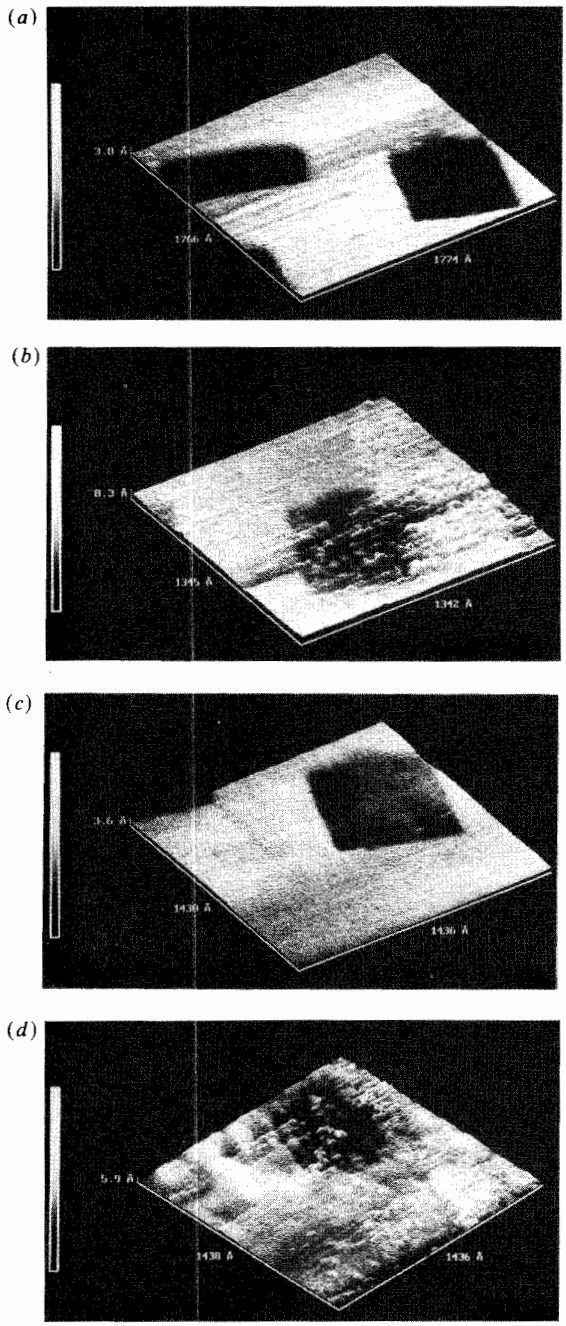


**Fig. 8** Deposition of copper at the iodine-covered Pt(100) surface from $10^{-3}$ mol dm$^{-3}$ $CuSO_4$, $10^{-2}$ mol dm$^{-3}$ $H_2SO_4$. Topographic images obtained with a Pt–Ir tip. Scan speed 300 nm s$^{-1}$. (*a*) Before deposition, at 0.2 V *vs.* $Cu/Cu^{2+}$, tunnelling voltage +85 mV. (*b*) After deposition at −0.2 V, image obtained under open-circuit conditions, tunnelling voltage +16 mV. (*c*) After dissolution of Cu at 0.2 V, tunnelling voltage 100 mV. (*d*) After another deposition at −0.2 V, image obtained under open-circuit conditions, tunnelling voltage 16 mV

minimize the shielding of the electrode at the position of the tip. After deposition of copper corresponding to 13 monolayers, the electrode was imaged again at open circuit [Fig. 8(*b*)]. While the monoatomic steps are still visible, copper is deposited in islands with a diameter of 30 Å and a height of two monolayers. No preferential deposition of the monoatomic steps could be observed. The island height of two monolayers suggests that Cu deposition does not take place *via* a layer-by-layer, but rather a three-dimensional growth. It must be kept in mind, however, that the shielding effect of the tip is still substantial, since the amount of copper visible in the islands is much less than the 13 monolayers deposited. The size of the islands is similar to that found by Kolb and co-workers after Cu deposition on Au electrodes.[16]

After dissolution of the copper at +200 mV an image similar to that of Fig. 8(*a*) is obtained [Fig. 8(*c*)]. Repeating the procedure, this time depositing an overall amount of copper corresponding to 22 monolayers, leads to the image shown in Fig. 8(*d*). The monoatomic steps of the substrate are still visible, but instead of finite islands the deposited copper now forms a broad hill-like structure.

In a separate experiment, only one monolayer (besides the Cu UPD) was deposited at an overpotential of −100 mV. Islands with a monoatomic height were formed having a diameter of 15 Å. Again no preferential deposition at steps of the substrate was found.

## Conclusions

*In situ* scanning tunnelling microscopy is able to reveal real space structures of electrochemical surfaces. This is true both for three-dimensional structures as formed by electrodeposition and for two-dimensional adsorbate systems.

Whereas closely packed, well ordered adsorbate species such as the Pt(100) $\sqrt{2}\times 5\sqrt{2}-$I adlayer can be imaged with a very good resolution, we always obtained worse resolutions at domain boundaries (Fig. 3 is an exception) and for less densely packed and less ordered iodine adlayers. This is probably caused by thermal movements and, as exemplified in Fig. 2, by movements of adatoms caused by the interaction with the tip. This problem might be even more drastic for adsorbate systems which are less strongly adsorbed.

Whereas at a potential of 1 V, the Pt(100) $(\sqrt{2}\times 5\sqrt{2})$R45°−I adlattice ($\theta = 0.6$) seems to be the only possible structure, at 0.5 V this structure coexists with a $(\sqrt{2}\times\sqrt{2})$R45°−I adlattice ($\theta = 0.5$). Complete desorption of the iodine at 0.25 V causes the Pt(100) surface to reconstruct and form a hexagonal overlayer.

Copper deposition onto the iodine-covered Pt(100) surface proceeds *via* a three-dimensional island growth.

Thanks are due to the DFG and AGEF for financial support.

## References

1 A. Wieckowski, S. D. Rosasco, B. C. Schardt, J. C. Stickney and A. T. Hubbard, *Inorg. Chem.*, 1984, **23**, 565.
2 D. Zurawski, L. Rice, M. Hourani and A. Wieckowski, *J. Electroanal. Chem.*, 1987, **230**, 221.
3 B. C. Schardt, S. L. Yau and F. Rinaldi, *Science*, 1989, **243**, 981.
4 R. Vogel, I. Kamphausen and H. Baltruschat, *Ber. Bunsenges. Phys. Chem.*, 1992, **96**, 525.
5 R. Vogel and H. Baltruschat, *Surf. Sci. Lett.*, 1991, **259**, L739; *Ultramicroscopy*, 1992, **42–44**, 562.
6 G. J. Cali, G. M. Berry, M. E. Bothwell and M. P. Soriaga, *J. Electroanal. Chem.*, 1991, **297**, 523.
7 J. Clavilier, R. Faure, G. Guinet and R. Durand, *J. Electroanal. Chem.*, 1980, **272**, 205.
8 D. Armand and J. Clavilier, *J. Electroanal. Chem.*, 1989, 331.
9 S-L. Yau, C. M. Vitus and B. C. Schardt, *J. Am. Chem. Soc.*, 1990, **112**, 3677.
10 C. M. Vitus, S-C. Chang, B. C. Schardt and M. J. Weaver, *J. Phys. Chem.*, 1991, **95**, 7559.
11 F. Lu, G. M. Salaita, H. Baltruschat and A. T. Hubbard, *J. Electroanal. Chem.*, 1987, **222**, 305.
12 J. L. Stickney, S. D. Rosasco, B. C. Schardt and A. T. Hubbard, *J. Phys. Chem.*, 1984, **88**, 251.

13 K. Besocke, *Surf. Sci.*, 1987, **181**, 145.
14 T. Michely, K. H. Besocke and M. Teske, *J. Microsc.*, 1988, **152**, 77.
15 X. Gao, A. Hamelin and M. J. Weaver, *Phys. Rev. Lett.*, 1991, **67**, 618.
16 R. J. Nichols, D. M. Kolb and R. J. Behm, *J. Electroanal. Chem.*, 1991, **313**, 109.

*Paper* 2/02739I; *Received* 26*th May*, 1992